Free Energy Profiles for the Identity S_N2 Reactions $Cl^- + CH_3Cl$ and $NH_3 + H_3BNH_3$: A Constraint *Ab Initio* Molecular Dynamics Study

Sheng-Yong Yang, Paul Fleurat-Lessard, Iordan Hristov, and Tom Ziegler*

Department of Chemistry, University of Calgary, University Drive 2500, Calgary, Alberta, Canada T2N 1N4

Received: July 9, 2004; In Final Form: August 17, 2004

Density functional theory (DFT) together with Car-Parrinello *ab initio* molecular dynamics (CP-AIMD) simulation has been used to investigate the free energy profiles of two representative S_N2 reactions: (A) $Cl^- + CH_3Cl \rightarrow ClCH_3 + Cl^-$; (B) $NH_3 + H_3BNH_3 \rightarrow H_3NBH_3 + NH_3$. The free energy profiles along the reaction coordinates at 300 K and 600 K were determined directly by a pointwise thermodynamic integration (PTI) technique. Comparison between the well-known double-well potential energy profile (PEP) and the free energy profiles (FEP) has been made. The results show that, for reaction A, the double-well profile is maintained for the FEP at 300 K due to the stronger ion−dipole interaction between chloromethane and the chloride anion. In comparison with the PEP, the FEP has a higher central barrier and a more shallow well depth. However, at 600 K the double wells almost disappear on the FEP, whereas the central barrier increases further. For reaction B, the 300 K FEP also presents a higher central barrier peak and a more shallow well depth compared to the PEP. However, when the temperature increases to 600 K, a saddle shape FEP is obtained, which indicates that the reaction has changed mechanism from an associative S_N2 reaction to a dissociative S_N1 reaction. This change is driven by entropy.

Introduction

The bimolecular nucleophilic substitution (S_N2) process is an important elementary reaction step in organic chemistry that has been extensively studied both experimentally[1−5] and theoretically.[6−12] Of special interest is the identity S_N2 reaction (eq 1) that has served as the starting model for the understanding of more complex substitution reactions in which the incoming and outgoing groups are different.

$$X + RX \rightarrow XR + X \qquad (1)$$

It is well established[13,14] that the potential energy profile for the reaction in eq 1 has the shape of a symmetric double well; see Chart 1. The minima in Chart 1 correspond to the prereaction complex X···RX and the postreaction complex XR···X, which are separated by a central energy barrier ΔE^B(X···R···X). The overall reaction process starts from a collision step, which generates the prereaction complex X···RX, and passes through a chemical activation step to overcome a transition state (TS) barrier. Once the TS has been reached and the associated barrier surmounted, a postreaction complex is formed followed by dissociation to generate the product. The profile in Chart 1 can thus be characterized by two parameters. One is the complexation energy ΔE^C defined as the difference between the prereaction/postreaction complex and reactants. The other one is the barrier height ΔE^B or the intrinsic barrier ΔE^{IB}, taken relative to the reactants and the intermediate complex, respectively.

Much progress has been achieved in determining and analyzing the potential energy surface[13,15,16] for the reaction of eq 1 in the gas phase. However, a few aspects still remain unexplored with respect to the reaction in eq 1. One is the determination of the entropy change along the reaction path in order to establish the corresponding free energy profile. Another aspect is the possibility for an alternative reaction path at higher temperatures. Thus, although the double-well-potential mechanism with its two intermediates representing prereaction and postreaction complexes is now generally accepted, a direct exchange for the reaction $Cl^- + CH_3Cl \rightarrow ClCH_3 + Cl^-$, in which pre- and postreaction complexes have very short lifetimes, has been found by Hase and co-workers[17] using classical trajectory calculations.

CHART 1

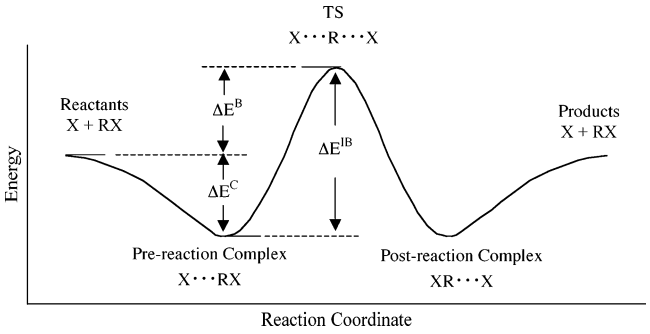

The calculation of a free energy profile can be accomplished within the harmonic approximation by evaluating the potential energy Hessian for all degrees of freedom perpendicular to a chosen path. Alternatively use can be made of *ab initio* molecular dynamics (AIMD) in conjunction with umbrella sampling,[18,19] the free energy perturbation method, or thermodynamic integration.[20−22] Here we adopt the thermodynamic integration method.

In the present study we explore the free energy profiles for two representative identity S_N2 reactions: (A) $Cl^- + CH_3Cl \rightarrow ClCH_3 + Cl^-$; (B) $NH_3 + H_3BNH_3 \rightarrow H_3NBH_3 + NH_3$. The objective here has been to explore differences in the shapes of the potential energy and free energy profiles as well as the

* To whom correspondence should be addressed. E-mail: zielger@ucalgary.ca.

10.1021/jp046954j CCC: $27.50
Published on Web 09/29/2004

CHART 2

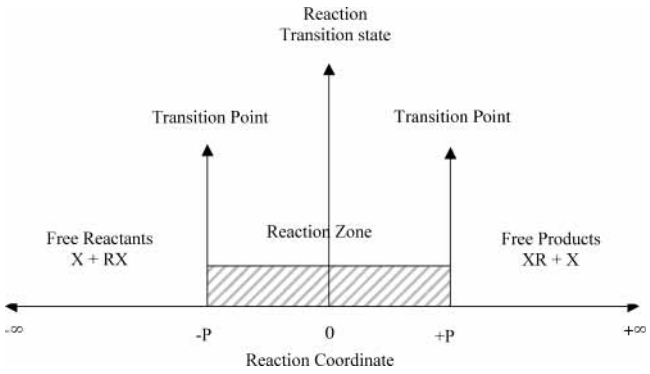

possibility for alternative reaction paths at higher temperatures. Please note that in this study we just consider the back-side reaction mode although the possible front-side reaction mechanism with a much higher energy barrier has been studied both experimentally and theoretically.[23−25]

Methodology and Computational Details

A. Thermodynamic Integration. Within a canonical (NVT) ensemble, the change in the Helmholtz free energy ΔA between two states *a* and *b* is given according to the thermodynamic integration method as

$$\Delta A_{a\rightarrow b} = \int_a^b \left\langle \frac{\partial E(X,s)}{\partial s} \right\rangle_s \mathrm{d}s = -\int_a^b \langle F_s \rangle \, \mathrm{d}s \qquad (2)$$

Here *s* is a running parameter for the progress along the reaction coordinate, *E* represents the potential energy of the system as a function of the 3*N* spatial coordinates, *X*, with the constraint *s*. Further, F_s is the force acting on the chosen constraint. The brackets indicate an ensemble average of the system at the constraint value *s*. Here we should mention that the simple formula in eq 1 is correct just for certain types of reaction coordinate including those used here. An accurate and much more complicated formula that can be applied to any general reaction coordinate can be found in refs 22 and 26. The integral of eq 2 is typically evaluated through a finite difference numerical integration scheme referred to as pointwise thermodynamic integration (PTI).[27] In the PTI scheme, a small number of points along the reaction coordinate are chosen, and the system is allowed to dynamically evolve and sample phase space at each point for a long time with no data collected between each point. The average force at each point is then used as the ensemble average of the force in eq 2. A slow growth continuous variation of the reaction coordinate has also been used to monitor the variation in the other degrees of freedom along the reaction coordinate.

For the purpose of studying the whole reaction process from reactants to products, the differences of the bond distances $R(Cl_1-C)$ and $R(C-Cl_2)$ for A, and $R(N_1-B)$ and $R(B-N_2)$ for B, have been defined as the reaction coordinates (here, atoms with subscripts 1 and 2 represent the attacking and leaving atoms respectively).

B. Transition Point and Reaction Zone. We introduce here the concepts of transition point and reaction zone to facilitate the later discussion.

We assume that the attacking nucleophile X approaches RX from infinite distance. The two molecules X and RX can move (translate and rotate) freely for large positive/negative values of the reaction coordinate (RC) where the intermolecular interaction is negligible (see the left part of Chart 2). Thus, in this region the X and RX species can be considered as two separated or isolated molecules. When the two molecules approach close enough to each other, their interaction will not be negligible, and the two molecules start to react. This area is referred to as the reaction zone (see the central part of Chart 2). We can imagine that there must exist one transition point (not exactly a point, possibly a small area) along the reaction coordinate, from which the system goes into the reaction zone. At this point, the free rotation of the two reacting species will start to be hindered and the intermolecular interaction has to be considered (see "−P" of Chart 2). The transition point can be obtained approximately by monitoring the change in energy with the reaction coordinate. We shall in the following associate the transition point with the RC values where $\mathrm{d}E/\mathrm{d}RC \approx 5 \times 10^{-4}$ hartree/bohr.[28]

The dynamic simulations and the calculations of the free energy profile will start and end just outside the transition points.

C. Free Energy Corrections. In our dynamic simulations, another two constraints were applied to the system on top of the reaction coordinate. First, no translation of the center of mass of the whole system was allowed. Second, rotation of the total system about the center of mass was eliminated. Thus, to get the correct FEP, the entropy contributions to the reaction free energy from the translation and rotation of the whole system have to be added.

We followed the correction scheme used by Kelly et al.[29] Thus, for the identity S_N2 reactions studied here, symmetry allows us to consider only the first part from RC = −∞ (infinite) to RC = 0 (transition state). The overall entropy correction from isolated reactants to a reaction coordinate of *s* is

$$\Delta S^{AB}_{PAWcorr}(s) = S^{AB}_r(s) + S^{AB}_T(s) - S^{A}_T(\infty) - S^{B}_T(\infty) \qquad (3)$$

where $S^{AB}_r(s)$ is the rotational entropy at RC = *s*, which is geometry dependent; $S^{AB}_T(s)$ the translational entropy at RC = *s*. The last two terms represent the translational entropy of the isolated species A and B. The translational/rotational entropy terms to the right in eq 3 can be calculated easily from the translational/rotational partition functions.

Finally, the total free energy change $\Delta A^{AB}_{CM}(s)$ is obtained from a Car-Parrinello projected augmented wave (CP-PAW) simulation with the constraints described above as

$$\Delta A^{AB}_{CM}(s) = \Delta A_{PAW}{}^{AB}(s) - T\Delta S_{PAWcorr}{}^{AB}(s) \qquad (4)$$

where CM (classical mechanics) refers to the fact that the motion of the nuclei is described using classical mechanics. Further, $\Delta A_{PAW}{}^{AB}(s)$ is the change in free energy obtained directly from the simulation using eq 2.

It should be mentioned that the zero point energy (ZPE) correction is not included in our simulations. This should not seriously hamper our objective, which is to understand the qualitative differences between the potential energy profile (PEP) and the free energy profile (FEP).

D. Density Functional and Molecular Dynamics Method. The Car-Parrinello projected augmented wave (CP-PAW)[30,31] program by Blöchl was used for all AIMD simulations. The DFT functional used was that formed by the combination of the Perdew−Wang parametrization of the electron gas[32] with the exchange gradient correction presented by Becke[33] and the correlation correction of Perdew.[34] Periodic boundary conditions were used, with a unit cell described by the lattice vectors ([0, 10, 10], [10, 0, 10], [18, 18, 0]) (Å) for the reaction $Cl^- + CH_3Cl$ and ([0, 12, 12], [12, 0, 12], [12, 12, 0]) (Å) for $NH_3 +$

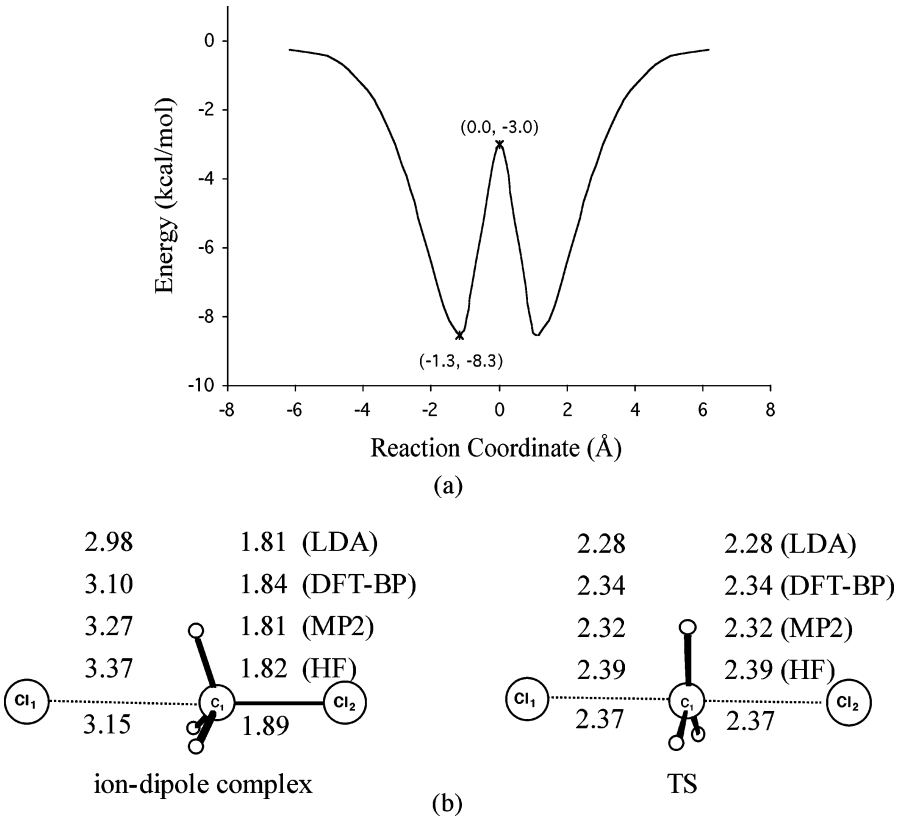

Figure 1. (a) Calculated potential energy profile for the S_N2 reaction $Cl^- + CH_3Cl \rightarrow ClCH_3 + Cl^-$ (energy of the isolated species is set to 0). (b) Key geometry parameters for the ion−dipole complex and the transition state. Bond distances in angstroms.

H_3BNH_3. These unit cells were sufficiently large to ensure negligible overlap of the wave functions with the periodic images. In all calculations the molecules have been electrostatically decoupled from their periodic images as described in ref 35. The energy cutoff used to define the basis set was 30 Ry (15 au) in all cases. The SHAKE algorithm[36] was used to impose constraints. The mass of hydrogen atoms was taken to be that of deuterium, and normal masses were taken for all other elements.

The CP-PAW calculations were performed at the two different target temperatures of 300 and 600 K. The Andersen thermostat[37] was applied to the nuclear motion by reassigning the velocity of N randomly chosen nuclei every n time steps, where N and n are chosen to maintain the desired temperature. In the case of chloromethane + chloride, the reassignment was applied every 18 time steps. The reaction $NH_3 + H_3BNH_3$ used one reassignment for every 15 time steps. The thermostat settings were monitored and adjusted if necessary during the equilibration stage, with the main criteria for adequate thermostating being that the mean temperature was within a range of ±15 K and the temperature drift was lower than 1 K/ps. In combination with the Andersen thermostat, a constant friction was applied to the wave function with a value of 0.003. For both reactions, a time step of 7 au was used.

The FEP does not directly provide information about the transition state structure except that the TS is situated at RC = 0. To obtain values for $R(Cl_1-C)$ and $R(C-Cl_2)$ for reaction A at the transition state, we carried out a molecular dynamics (MD) simulation in which both $R(Cl_1-C)$ and $R(C-Cl_2)$ were used as constraints. By changing the values of $R(Cl_1-C)$ and $R(C-Cl_2)$ such that the forces on the constraints were reduced, we finally reached the transition state as the point where the forces on the constraints $R(Cl_1-C) - R(C-Cl_2)$ and $R(Cl_1-C) + R(C-Cl_2)$ are both zero. During the optimization the Bofill Hessian update scheme[38] was used. A similar procedure was used to optimize the TS structure for reaction B. The results presented here represent the first application of a newly developed free energy gradient method[26] to the determination of transition state structures on the free energy surface.

Results and Discussion

A. $Cl^- + CH_3Cl \rightarrow ClCH_3 + Cl^-$. The chloride exchange reaction between chloromethane and the chloride anion, as a prototypical S_N2 reaction, has been studied extensively by many experimental and theoretical methods.[4,39−42] These studies have established a PEP similar to that shown in Chart 1 with a double-well shape where two minima are symmetrically situated around a central energy barrier. We present in the following the calculated PEP to compare to other theoretical results as well as the FEP. The PEP was obtained by changing the RC while optimizing all other degrees of freedom.

(a) Potential Energy Profile. A typical double well potential energy profile, shown in Figure 1a, has been obtained using the BP functional described before.[32−34] From Figure 1a, we can see that the internal energy is almost constant at RC < −6 Å. For RC > −6 Å, the potential energy begins to decrease until RC = −1.3 Å, which is an energy minimum corresponding to the ion−dipole complex. From RC = −1.3 Å to RC = 0.0 Å, the potential energy increases and finally reaches the maximum at the transition state. Clearly, on the potential energy surface, the reaction system goes into the reaction zone around RC = −6 Å.

The calculated complexation energy ΔE^C, the overall barrier ΔE^B relative to the reactants, and the intrinsic barrier ΔE^{IB} are given in Table 1 together with experimental and recent high-level theoretical results. We calculate a complexation energy of −8.3 kcal/mol and a central barrier given by −3.0 kcal/mol.

TABLE 1: Complexation Energies and Barrier Heights for the S_N2 Reaction $Cl^- + CH_3Cl \rightarrow ClCH_3 + Cl^-$ (in kcal/mol)

	ΔE^C	ΔE^B	ΔE^{IB}
CP-PAW-BP	−8.3	−3.0	5.4
HF[a]	−8.1	7.6	15.7
DFT-B3LYP[b]	−9.5	−0.9	8.7
DFT-BP[c]	−10.3	−5.7	4.6
MP2[a]	−10.5	3.5	14.0
MP4[c]	−10.6	1.8	12.4
G2[d]	−10.8	3.1	13.8
G3[d]	−11.2	1.8	13.0
CBS-QB3(+)[d]	−10.7	2.4	13.1
experiment[e]	−12 ± 2	3/1 ± 1	13 ± 2

[a] TZ3P+R+(2f,d) basis set, ZPE corrected, ref 43. [b] 6-31G* basis set, ZPE corrected, ref 44. [c] TZ+2P basis set, ZPE corrected, ref 25. [d] ZPE corrected, ref 40. [e] References 24 and 45−47.

If we compare our results (CP-PAW-BP) with Hartree−Fock,[43] DFT,[44] MP*n*,[25] G*n*, CBS-QB3(+),[40] and experimental results,[24,45−47] we find that MP2, MP4, G2, G3, and CBS-QB3-(+) afford more accurate estimates of both the complexation energy and the central barrier when compared to experiment. DFT-B3LYP and DFT-BP both afford negative values for the central barrier, whereas Hartree−Fock overestimates the central barrier by about 4 kcal/mol.

It is thus clear from Table 1 that most *ab initio* methods (MP*n*, G*n*, and CBS-QB3(+)) afford a better estimate of the PEP than DFT methods (DFT-B3LYP, DFT-BP, and CP-PAW-BP), which underestimate the internal barrier as well as the complexation energy. The main reason might be that the DFT method is not as good to accurately describe a transition state. However, we still hope that the CP-PAW-BP scheme used here will correctly provide the qualitative features for the entropic contribution ($-T\Delta S$) to the FEP and thus enable us to meet our key objective.

The optimized key geometry parameters for the transition state and the ion−dipole complex obtained from various methods are shown in Figure 1b. In the transition state, the two bond distances between chloride and carbon ($R(Cl_1-C)$ and $R(C-Cl_2)$) are equal at 2.37 Å for the CP-PAW-BP scheme, which is very close to the values of DFT-BP (2.34 Å), MP2 (2.32 Å),[25] and HF (2.39 Å).[43] In the ion−dipole complex, the $C-Cl_2$ bond distance is 1.89 Å according to the CP-PAW-BP scheme, which is comparable with results from LDA (1.81 Å),[25] DFT-BP (1.84 Å), MP2 (1.81 Å), and HF (1.82 Å). However significant differences are observed for the Cl_1-C distance in the ion−dipole complex. This is not surprising in view of the weak bonding interaction in the ion−dipole complex.

(b) 300 K Free Energy Profile. The calculated 300 K free energy profile along the reaction coordinate is shown in Figure 2a. It starts from the transition point where RC = −3.7 Å. It is apparent that the basic double-well shape is maintained on the FEP at 300 K.

However, four different features are noteworthy compared to the PEP: (1) The transition point shifts from RC = −6.0 Å to RC = −3.7 Å. Thus, until RC = −3.7 Å the chloromethane molecule and chloride ion are rotating freely (see below), overcoming the ion−dipole attraction. As a consequence, the free energy gradient is zero. This is different from the PEP, where the ion−dipole interaction already gives rise to an energy gradient at RC = −6.0 Å. (2) The central barrier ΔE^B has increased by +8.1 kcal/mol in going from 0 K (PEP) to 300 K (FEP). (3) The position of the minimum for the ion−dipole complex along the reaction coordinate has shifted from RC = −1.3 Å on the PEP to RC = −1.5 Å on the FEP. (4) The stability of the ion−dipole complex has decreased by 5.5 kcal/mol in going from 0 K (PEP) to 300 K (FEP). The difference between the two energy profiles is entropic in nature. As the ion−dipole complex is formed, the free rotation of CH_3Cl will be reduced (see below). This will lead to a reduction in entropy and an increase in $-T\Delta S$. The result is a reduction in the depth of the well for the ion−dipole complex on the FEP. A further reduction in entropy is observed at the transition state, where the rotation of CH_3Cl is completely converted into vibrations (see below). As a result, the TS barrier will encounter an additional increase up to 8.1 kcal/mol on the FEP relative to the PEP.

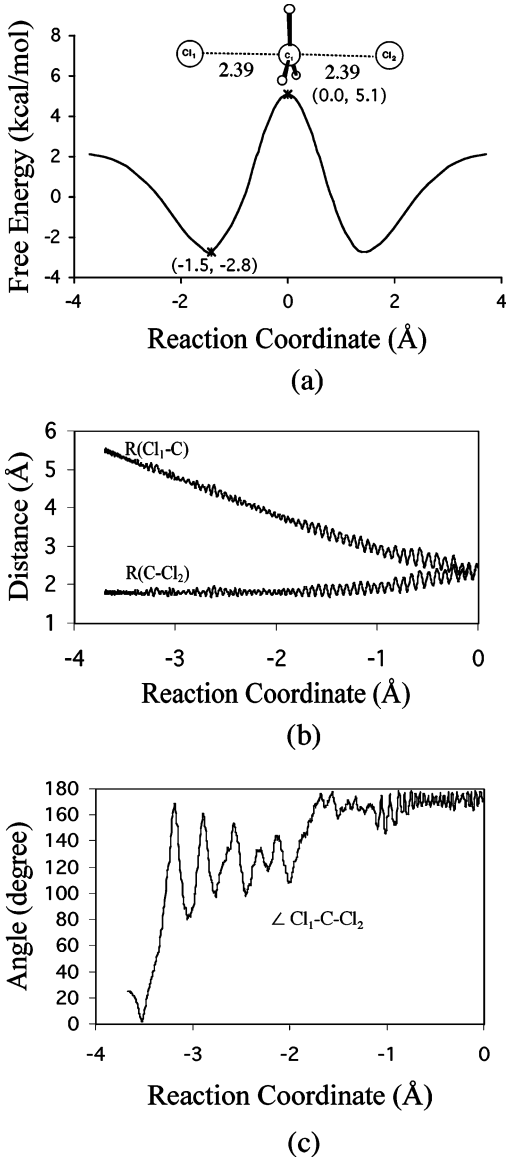

Figure 2. (a) Calculated free energy profile at 300 K with the transitional/rotational entropy corrected. Free energy ΔA is relative to the infinitely separated reactants. (b) Distance changes for $R(Cl_1-C)$ and $R(C-Cl_2)$ along the reaction coordinate. (c) Angle change for $\angle Cl_1-C-Cl_2$ along the reaction coordinate.

The calculated entropy change upon formation of the ion−dipole complex from the separated reactants is −18.3 eu at 300 K, in good agreement with the experimental estimate of −15.3 ± 1.0 eu due to Dougherty et al.[48] The entropy of the transition state is −27.0 eu relative to the separated reactants. The corresponding experimental number is not known. However, a DFT estimate based on the harmonic approximation affords −25.0 eu.[25]

The changes of the two key interatomic distances $R(Cl_1-C)$ and $R(C-Cl_2)$, as well as the angle Cl_1-C-Cl_2, from the MD simulation along the reaction coordinates are presented in Figure 2b,c. The simulation was started at RC = −3.7 Å, where the attacking chloride anion is 5.5 Å from the carbon. In the early stages of the reaction the incoming chloride (Cl_1) is approaching the carbon with little change in $R(C-Cl_2)$ while the CH_3Cl molecule is rotating as a rigid body around the $C-Cl_1$ axis in orbits where the Cl_1-C-Cl_2 angle has values from 180° to 80°. Thus, the rotation is somewhat restricted by the ion−dipole interaction, which has a minimum energy at $Cl_1-C-Cl_2 = 180°$. The point RC = −1.5 Å marks the formation of the ion−dipole complex. Shortly after that the Cl_1-C-Cl_2 angle turns toward 180° while the chloride anion continues to attack the carbon center and the leaving chloride starts to move until the transition state has been reached.

The transition state is a central feature of the S_N2 reactions. We have therefore located the key geometry parameters of the transition state on the free energy surface. The optimized distances $R(Cl_1-C)$ and $R(C-Cl_2)$ are 2.39 Å, which is longer than the corresponding value (2.37 Å) on the potential energy surface. To further examine the geometry changes with temperature, the same optimization has been performed at 600 K (the 600 K FEP will be discussed in detail later). The $R(Cl_1-C)$ and $R(C-Cl_2)$ values are 2.44 Å, and thus longer than those obtained at 300 K. These data reveal that, at finite temperatures up to at least 600 K, the transition state structures are symmetrical with $R(Cl-C)$ distances that increase with temperature. This bond length increase in the TS with temperature should be a common feature of the S_N2 reactions since the symmetrical Cl_1-C-Cl_2 stretch will be more and more thermally excited. The equilibrium distance will thus shift to longer values because of the nonharmonic contribution to the motion. This effect would not be observed by standard quantum mechanical methods based on the harmonic approximation.

(c) 600 K Free Energy Profile. To examine the temperature effect further, the 600 K free energy profile was calculated as well. Figure 3 displays the FEP and the changes in the key parameters $R(Cl_1-C)$, $R(C-Cl_2)$, and $<Cl_1-C-Cl_2$ along the reaction coordinate. Compared with results at 0 and 300 K, there are significant differences in the position of the transition point, the shape of the FEP, and the central barrier.

First of all, the free energy central barrier has increased to +20.5 kcal/mol compared to +5.1 kcal/mol at 300 K and −3.0 kcal/mol at 0 K. Clearly the decrease in entropy results in the increase in free energy at the transition state.

The starting point for the reaction zone at 600 K has shifted to RC = −3.1 Å compared to 6.0 Å at 0 K and −3.7 Å at 300 K. The higher thermal energy at 600 K makes CH_3Cl and Cl^- rotate freely until RC = −3.1 Å. This can be seen from Figure 3c, where the Cl_1-C-Cl_2 angle adopts values in the whole range between 0° and 180° until RC = −3.1 Å. In other words, up to RC = −3.1 Å the thermal energy overcomes any preferred orientations of CH_3Cl relative to Cl^- due to the ion−dipole interaction.

From RC = −3.1 Å to RC = −1.6 Å, the free rotation is gradually restricted until Cl_1-C-Cl_2 finally remains almost collinear; see Figure 3c. This restriction gives rise to a decrease in rotational entropy and an increase in free energy. On the other hand, the gradual alignment of the Cl_1-C and Cl_2-C bonds into a collinear arrangement leads to a steady (stabilizing) increase in the ion−dipole interaction. The transition from stabilization due to rotational entropy to stabilization due to ion−dipole interaction give rise to a small barrier near RC = −2.1 Å. Finally, the FEP exhibits a minimum at RC = −1.6 Å representing the ion−dipole complex. However, it is clear from our analysis at $T = 600$ K that the double well representing the ion−dipole complexes will disappear at higher temperatures.

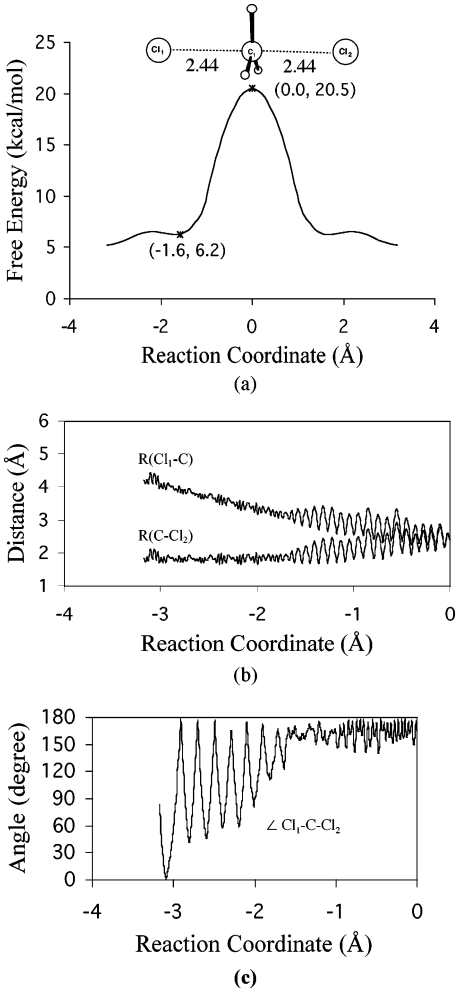

Figure 3. (a) Calculated free energy profile at 600 K with the transitional/rotational entropy corrected. Free energy ΔA is relative to the infinitely separated reactants. (b) Distance changes for $R(Cl_1-C)$ and $R(C-Cl_2)$ along the reaction coordinate. (c) Angle change for $\angle Cl_1-C-Cl_2$ along the reaction coordinate.

B. $NH_3 + H_3BNH_3 \rightarrow H_3NBH_3 + NH_3$. S_N2 reactions involving four-coordinated and tetrahedron boron are of special interest because they may compete with S_N1 pathways in which relatively stable three-coordinated boron compounds are formed.[49−51] Such three-coordinated species are not likely to form in substitution reactions involving carbon. Especially one can expect that the entropy at higher temperatures would change the substitution around four-coordinated boron from an associative S_N2 mechanism to a dissociative S_N1 mechanism.

The reaction comprised of borane (BH_3) and ammonia (NH_3) was chosen as our model system representing a substitution at the boron center. Toyota et al.[51] have calculated the reaction barriers for the possible S_N2 and S_N1 mechanisms for system B by static *ab initio* methods (HF/MP2/MP3). They found that the S_N2 mechanism had a barrier that was 19.3 kcal/mol lower than the S_N1 pathway. Here we shall focus on the possible differences between PEP and FEP, as well as the temperature effect on the mechanism. Therefore, we will again explore the PEP and the FEP at 300 and 600 K using the same method.

(a) Potential Energy Profile. The calculated PEP of reaction B, as well as several key species along the reaction coordinate

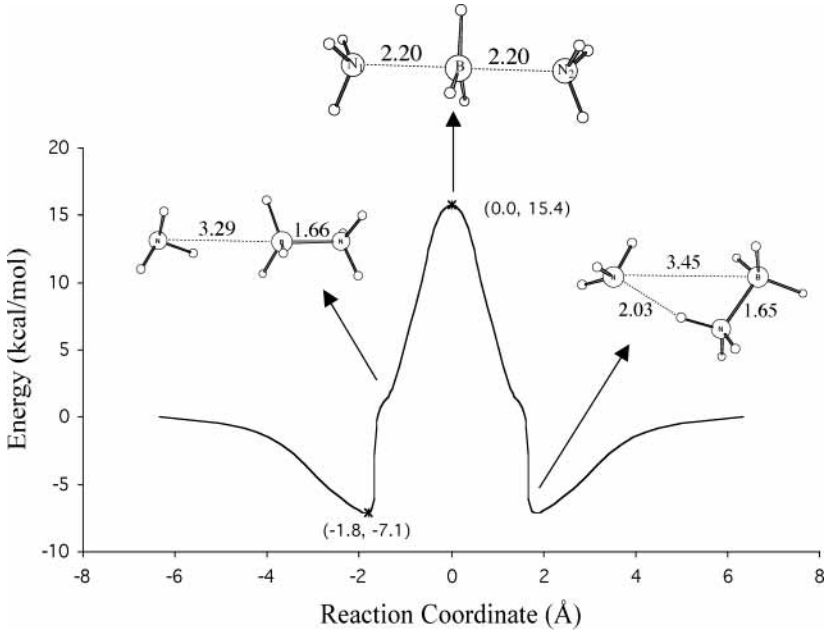

Figure 4. Calculated potential energy profile for the S_N2 reaction $NH_3 + H_3BNH_3 \rightarrow H_3NBH_3 + NH_3$ with structures of transition state and two intermediates (distances in angstroms).

RC = $R(N_2-B) - R(N_1-B)$, are displayed in Figure 4. The reaction starts from the point RC = −6.5 Å. Symmetrically around the central barrier at RC = ±1.6 Å is a small shoulder representing a *trans* $H_3N-BH_3-NH_3$ complex with the two B−N distances 1.66 and 3.29 Å. At RC = ±1.8 Å is another minimum representing a *cis* encounter complex in which the incoming and attacking NH_3 is hydrogen bonded to the other NH_3 that that is complexed to BH_3. The shorter N_1-H distance (2.03 Å) confirms the hydrogen bond between the two NH_3 groups. The central barrier ΔE^B is +15.4 kcal/mol with respect to the separated NH_3 and H_3BNH_3 species. Compared with the HF (+11.6 kcal/mol), MP2 (+13.6 kcal/mol), and MP3 (+13.8 kcal/mol) results by Toyota et al., our CP-PAW-BP scheme affords a somewhat high barrier. The transition state is represented by a symmetric structure with $R(N_1-B) = R(B-N_2)$ = 2.20 Å, which is shorter than the HF (2.43 Å), MP2 (2.22 Å), and MP3 (2.25 Å) distances.

(b) 300 K Free Energy Profile. The 300 K FEP, with a higher central barrier and two very shallow wells, is shown in Figure 5a. The central barrier has as expected increased relative to the zero baseline due to entropy and is now +18.5 kcal/mol compared to +15.4 kcal/mol for the PEP. On the other hand, the minimum for the hydrogen bonded *cis* encounter complex is reduced to only −1 kcal/mol.

The changes of the interatomic distances $R(N_1-B)$ and $R(B-N_2)$ and the angle N_1-B-N_2 along the reaction coordinate are displayed in Figure 5b,c. The simulation was started at RC = −3.5 Å, where the attacking N_1 (NH_3) center is a distance of 5.2 Å from the boron atom. From RC = −3.5 Å to RC = −1.6 Å, the incoming N_1 center is approaching the boron with little change in the $R(B-N_2)$ bond distance while the angle N_1-B-N_2 is around 50°. Thus, the reaction system is trapped in the hydrogen bond region (*cis* complex: $H_3N\cdots H_3NBH_3$). Starting from RC = −1.6 Å, the attacking N_1 center moves to the position *trans* to N_2 (H_3BNH_3). At this point the $R(B-N_2)$ distance begins to increase while the $R(N_1-B)$ bond length decreases still further. The reaction system finally reaches the symmetric transition state at RC = 0.0 Å.

Parameters for the optimized transition state are shown in Figure 5a. Compared with results from PEP, the interatomic distances between N and B are longer than those of PEP by 0.06 Å. Following the result from reaction A, the N−B distance

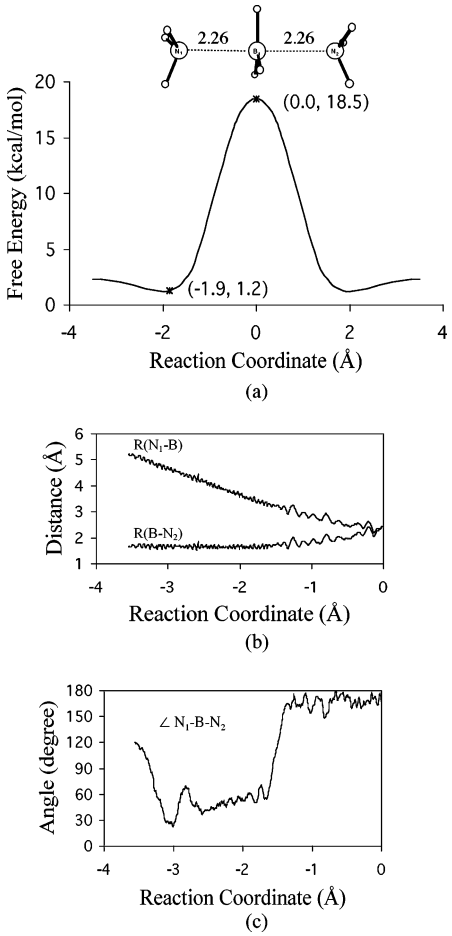

Figure 5. (a) Calculated free energy profile for the S_N2 reaction $NH_3 + H_3BNH_3 \rightarrow H_3NBH_3 + NH_3$ at 300 K with the transitional/rotational entropy corrected. Free energy ΔA is relative to the infinitely separated reactants. (b) Distance changes for $R(N_1-B)$ and $R(B-N_2)$ along the reaction coordinate. (c) Angle change for $\angle N_1-B-N_2$ along the reaction coordinate.

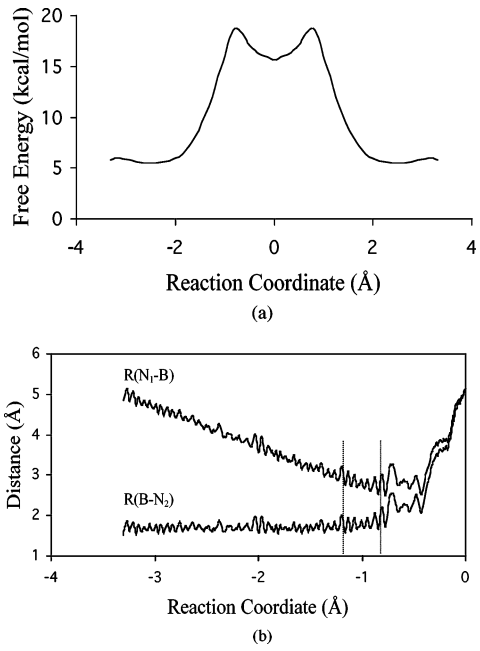

Figure 6. (a) Calculated free energy profile for the reaction $NH_3 + H_3BNH_3 \rightarrow H_3NBH_3 + NH_3$ at 600 K with the transitional/rotational entropy corrected. Free energy ΔA is relative to the infinitely separated reactants. (b) Distance changes for $R(N_1-B)$ and $R(B-N_2)$ along the reaction coordinate.

in the transition state for reaction B should elongate with increasing temperature. Nevertheless if the N−B distance becomes long enough, the H_3NBH_3 molecule would probably prefer to dissociate into NH_3 and BH_3 since BH_3 is stable by itself and the dissociation is favored by entropy. Thus rationally we can imagine that it is possible for the mechanism of the nucleophilic substitution reaction at the four-coordinated boron system to change at high temperatures.

(c) 600 K Free Energy Profile. Efforts have been made to calculate the free energy profile at 600 K. We obtained an FEP with a double-peak shape, as depicted in Figure 6a, which is a typical energy profile for a classical dissociative S_N1 process. To understand fully the mechanism, two further examinations have been made.

First, a number of constraint MD simulations around RC = 0.0 Å have been analyzed. The results revealed that at this point the system consists of three separated molecules, i.e., two NH_3 and one BH_3 molecules.

Second, simulations with a slow growth continuous variation of the reaction coordinate from RC = −3.3 Å (starting point) to RC = 0.0 Å have been performed. The changes of the bond distances $R(N_1-B)$ and $R(B-N_2)$ along the reaction coordinate are displayed in Figure 6b. Clearly, from RC = −3.3 Å to RC = −1.2 Å, the N_1-B distance decreases linearly and the $B-N_2$ bond length remains almost unchanged. In the region with −1.2 Å < RC < −0.8 Å, the $B-N_2$ distance starts to increase and the N_1-B bond length continues to decrease. Thus, until RC = −0.8 Å, the process is quite similar to that of the S_N2 mechanism discussed before. However, when RC > −0.8 Å, the situation changes. Although N_2 (NH_3) keeps moving away from the boron center, the N_1 (NH_3) stops approaching the B (BH_3) any further. First the N_1-B equilibrium distance remains at the value of ca. 3.0 Å for a short time. Then N_1 begins to leave boron rapidly, which is concomitant with the quick breaking of the $B-N_2$ bond. Finally the reaction system becomes three separate molecules around RC = 0.0 Å. Accordingly, the process starting from RC = −0.8 Å to RC = 0.0 Å is very similar to the classical dissociative S_N1 process.

Apparently the process for reaction B at 600 K, in which the attacking nucleophile NH_3 approaches the boron center and then both the leaving NH_3 and attacking NH_3 dissociate, does not follow the classical dissociative S_N1 process exactly. However, from another point of view, we know that the nucleophile N_1 (NH_3) approaching the boron center can assist in the breaking of the $B-N_2$ bond. Indeed the calculated free energy barrier for the dissociation of H_3B-NH_3 without the assistance of an additional NH_3 molecule at 600 K[52] is ca. 5 kcal/mol higher than that in which an additional NH_3 molecule assists. Thus, we can say that the mechanism of reaction B at 600 K is a nucleophilically (NH_3) assisted S_N1 process.

Conclusions

The free energy profiles of two typical S_N2 reactions (A) $Cl^- + CH_3Cl \rightarrow ClCH_3 + Cl^-$ and (B) $NH_3 + H_3BNH_3 \rightarrow H_3NBH_3 + NH_3$ have been obtained from Car-Parrinello *ab initio* molecular dynamics (CP-AIMD) simulations. The free energy along the reaction coordinates at 300 and 600 K were determined directly by the pointwise thermodynamic integration (PTI) technique. Comparison between the potential energy profiles (PEP) and the free energy profile (FEP) has been made. The results show that reaction A has a typical double-well PEP with a −3.0 kcal/mol central barrier and a well depth of −8.3 kcal/mol for the ion pair pre- and postreaction complexes. The double-well shape is maintained very well for the FEP at 300 K because of the stronger ion−dipole interaction between chloromethane and the chloride anion. In comparison with the PEP, the FEP at 300 K has a higher central barrier and lower well depth for the ion−dipole complex. However, at 600 K the double well almost disappears on the FEP, while the central barrier increases. For reaction B, the 300 K FEP presents a much higher central barrier peak (+18.5 kcal/mol) and a well depth of just −1.0 kcal/mol for the pre- and postreaction complexes. At 600 K a double-peak shape has been obtained for the FEP, which indicates that the reaction has now switched to a dissociative (S_N1) process driven by entropy.

Acknowledgment. We thank Dr. Michael Seth for helpful discussions. This work was supported by the National Sciences and Engineering Research Council of Canada (NSERC). Calculations were performed in part on the Westgrid cluster and the MACI Alpha cluster located at the University of Calgary. T.Z. thanks the Canadian government for a Canada Research Chair. I.H. thanks the Alberta Ingenuity Fund for their support.

References and Notes

(1) Le Garrec, J.-L.; Rowe, B. R.; Queffelec, J. L.; Mitchell, J. B. A.; Clary, D. C. *J. Chem. Phys.* **1997**, *107*, 1021.

(2) Seeley, J. V.; Morris, R. A.; Viggiano, A. A.; Wang, H.; Hase, W. L. *J. Am. Chem. Soc.* **1997**, *119*, 577.

(3) DeTuri, V. F.; Hintz, P. A.; Ervin, K. M. *J. Phys. Chem. A* **1997**, *101*, 5969.

(4) Chabinyc, M. L.; Craig, S. L.; Regan, C. K.; Brauman, J. I. *Science* **1998**, *279*, 1882.

(5) Craig, S. L.; Brauman, J. I. *J. Phys. Chem. A* **1997**, *101*, 4745.

(6) Gonzales, J. M.; Pak, C.; Cox, R. S.; Allen, W. D.; Schaefer, H. F., III; Csaszar, A. G.; Tarczay, G. *Chem. Eur. J.* **2003**, *9*, 2173.

(7) (a) Baer, T.; Hase, W. L. In *Unimolecular Reaction Dynamics—Theory and Experiments*; Oxford: New York, 1996. (b) Wang, H.; Goldfield, E. M.; Hase, W. L. *J. Chem. Soc., Faraday Trans.* **1997**, *93*, 737. (c) Wang, H.; Hase, W. L. *Chem. Phys.* **1996**, *212*, 247.

(8) Botschwina, P.; Horn, M.; Seeger, S.; Oswald, R. *Ber. Bunsen-Ges. Phys. Chem.* **1997**, *101*, 387.

(9) Clary, D. C.; Palma, J. *J. Chem. Phys.* **1996**, *106*, 575.

(10) (a) Glukhovtsev, M. N.; Pross, A.; Radom, L. *J. Am. Chem. Soc.* **1996**, *118*, 6273. (b) Glukhovtsev, M. N.; Pross, A.; Radom, L. *J. Am. Chem. Soc.* **1995**, *117*, 2024.

(11) Hu, W.-P.; Truhlar, D. G. *J. Am. Chem. Soc.* **1995**, *117*, 10726.

(12) (a) Tachikawa, H. *J. Phys. Chem. A* **2001**, *105*, 1260. (b) Tachikawa, H. *J. Phys. Chem. A* **2002**, *104*, 497.

(13) Shaik, S. S.; Schlegel, H. B.; Wolfe, S. *Theoretical Aspects of Physical Organic Chemistry: The S_N2 Mechanism*; John Wiley & Sons: New York, 1992.

(14) (a) Olmstead, W. N.; Brauman, J. I. *J. Am. Chem. Soc.* **1977**, *99*, 4219. (b) Barfknecht, A.; Dodd, J. A.; Salomon, K. E.; Tumas, W. E.; Brauman, J. I. *Pure Appl. Chem.* **1984**, *56*, 1809.

(15) Parthiban, S.; Oliveira, G.; Martin, J. M. L. *J. Phys. Chem. A* **2001**, *105*, 895.

(16) Tucker, S. C.; Truhlar, D. G. *J. Phys. Chem.* **1989**, *93*, 8138.

(17) Vande, S. R.; Hase, W. L. *J. Am. Chem. Soc.* **1989**, *111*, 2349.

(18) Frenkel, D.; Smit, B. *Understanding Molecular Simulation*; Academic: San Diego, CA, 1996.

(19) Van Gunsteren, W. F.; Beutler, T. C.; Fraternali, F.; King, P. M.; Mark, A. E.; Smith, P. E. In *Computer Simulation of Biomolecular Systems: Theoretical and Experimental Applications*; Van Gunsteren, W. F., Weiner, P., Wilkinson, A. J., Eds.; ESCOM: Leiden, The Netherlands, 1993; Vol. 2, p 315.

(20) Carter, E. A.; Ciccotti, G.; Hynes, J. T.; Kapral, R. *Chem. Phys. Lett.* **1989**, *156*, 472.

(21) Paci, E.; Ciccotti, G.; Ferrario, M.; Kapral, R. *Chem. Phys. Lett.* **1991**, *176*, 581.

(22) (a) Den Otter, W. K.; Briels, W. J. *J. Chem. Phys.* **1998**, *109*, 4139. (b) Sprik, M.; Ciccotti, G. *J. Chem. Phys.* **1998**, *109*, 7737. (c) Den Otter, W. K.; Briels, W. J. *Mol. Phys.* **2000**, *98*, 773. (d) Darve, E.; Pohorille, A. *Mol. Simul.* **2002**, *28*, 113. (e) Darve, E.; Pohorille, A. *J. Chem. Phys.* **2001**, *115*, 9169. (f) Schlitter, J.; Klähn, M. *Mol. Phys.* **2003**, *101*, 3439.

(23) Glukhovtsev, M. N.; Pross, A.; Schlegel, H. B.; Bach, R. D.; Radom, L. *J. Am. Chem. Soc.* **1996**, *118*, 11258.

(24) Barlow, S. E.; Van Doren, J. M.; Bierbaum, V. M. *J. Am. Chem. Soc.* **1988**, *110*, 7240.

(25) Deng, L.; Branchadell, V.; Ziegler, T. *J. Am. Chem. Soc.* **1994**, *116*, 10645.

(26) Fleurat-Lessard, P.; Ziegler, T. Manuscript in preparation.

(27) Straatsma, T. P.; McCammon, J. A. *J. Chem. Phys.* **1991**, *95*, 1175.

(28) Actually, the energy gradient and the maximum of the free energy could be used to define the transition point. However, the energy gradient, other than the free energy, could be obtained directly from the dynamic simulation. We expected that it should be more reliable and easier to manage if the energy gradient was used to define the transition point.

(29) Kelly, E.; Seth, M.; Ziegler, T. *J. Phys. Chem. A* **2004**, *108*, 2167.

(30) Blöchl, P. E. *Phys. Rev. B* **1994**, *50*, 17953.

(31) Blöchl, P. E. *J. Phys. Chem.* **1995**, *99*, 7422.

(32) Perdew, J. P.; Wang, Y. *Phys. Rev. B* **1992**, *45*, 13244.

(33) Becke, A. *Phys. Rev. A* **1988**, *38*, 3098.

(34) Perdew, J. P. *Phys. Rev. B* **1986**, *33*, 8822.

(35) Blöchl, P. E. *J. Chem. Phys.* **1995**, *103*, 7422.

(36) Ryckaert, J. P.; Cicotti, G.; Berensden, H. J. *J. Comput. Phys.* **1977**, *23*, 327.

(37) Andersen, H. C. *J. Chem. Phys.* **1980**, *72*, 2384.

(38) Bakken, V.; Millam, J. M.; Schlegel, H. B. *J. Chem. Phys.* **1999**, *111*, 8773.

(39) (a) Hase, W. L. *Science* **1994**, *266*, 998. (b) Sun, L.; Hase, W. L.; Song, K. *J. Am. Chem. Soc.* **2001**, *123*, 5753. (c) Li, G.; Hase, W. L. *J. Am. Chem. Soc.* **1999**, *121*, 7124.

(40) Parthiban, S.; Oliveira, G. D.; Martin, J. M. L. *J. Phys. Chem. A* **2001**, *105*, 895.

(41) Ensing, B.; Meijer, E. J.; Blöchl, P. E.; Baerends, E. J. *J. Phys. Chem. A* **2001**, *105*, 3300.

(42) Merkel, A.; Havlas, Z.; Zahradnik, R. J. *Am. Chem. Soc.* **1988**, *110*, 8355.

(43) Wladkowski, B. D.; Lim, K. F.; Allen, W. D.; Brauman, J. I. *J. Am. Chem. Soc.* **1992**, *114*, 9136 and references therein.

(44) Streitwieser, A.; Choy, G. S.; Abu-Hasanayn, F. *J. Am. Chem. Soc.* **1997**, *119*, 5013.

(45) Larson, J. W.; McMahon, T. B. *J. Am. Chem. Soc.* **1985**, *107*, 766.

(46) Li, C.; Ross, P.; Szulejko, J. E.; McMahon, T. B. *J. Am. Chem. Soc.* **1996**, *118*, 9360.

(47) Wladkowski, B. D.; Brauman, J. I. *J. Phys. Chem.* **1993**, *97*, 13158.

(48) (a) Dougherty, R. C.; Dalton, J.; Roberts, J. D. *Org. Mass Spectrom.* **1974**, *8*, 77. (b) Dougherty, R. C.; Roberts, J. D. *Org. Mass Spectrom.* **1974**, *8*, 81. (c) Dougherty, R. C. *Org. Mass Spectrom.* **1974**, *8*, 85.

(49) Walmsley, D. E.; Budde, W. L.; Hawthorne, M. F. *J. Am. Chem. Soc.* **1971**, *93*, 3150.

(50) Black, D. St. C. *Comprehensive Coordination Chemistry*; Wilkinson, G., Gillard, R. D., McCleverty, J. A., Eds.; Pergamon: Oxford, 1987; Vol. 6.

(51) Toyota, S.; Futawaka, T.; Asakura, F. M.; Ikeda, H.; Oki, M. *Organometallics* **1998**, *17*, 4155.

(52) The same method was used to calculate the H_3B-NH_3 dissociation process at 600 K. The calculated free energy barrier is ca. 18.5 kcal/mol.